New Mechanism for Long Photo-Induced Enhanced Raman Spectroscopy in Au Nanoparticles Embedded in TiO 2

Andrea Brognara, Beatrice R Bricchi, Ludovic William, Ovidiu Brinza, Maria Konstantakopoulou, Andrea Li Bassi, Matteo Ghidelli, Nathalie Lidgi-Guigui

New mechanism for long Photo-Induced Enhanced Raman Spectroscopy in Au nanoparticles embedded in TiO_2

*Andrea Brognara[1,2], Beatrice R. Bricchi[1], Ludovic William[3], Ovidiu Brinza[3], Maria Konstantakopoulou[3], Andrea Li Bassi[1], Matteo Ghidelli[123], Nathalie Lidgi-Guigui[3]**

[1] Dipartimento di Energia, Micro and Nanostructured Materials Laboratory, Politecnico di Milano, via Ponzio 34/3, I-20133, Milano, Italy

[2] Department of Structure and Nano/-Micromechanics of Materials, Max-Planck-Institut für Eisenforschung GmbH, Max-Planck-Straße 1, 40237 Düsseldorf, Germany

[3] Laboratoire des Sciences des Procédés et des Matériaux (LSPM), CNRS,
Université Sorbonne Paris Nord, 93430, Villetaneuse, France

*nathalie.lidgi-guigui@univ-paris13.fr

Keywords: TiO_2; SERS; nanoparticles; cathodoluminescence; photo-induced charge separation; PIERS

Abstract.

The PIERS effect (Photo-Induced Enhanced Raman Spectroscopy) is a phenomenon taking place when plasmonic nanoparticles deposited on a semiconductor are illuminated by UV light before the Raman measurement. Recent results show enhancement of the Raman scattered intensity even greater that with conventional surface enhanced Raman Scattering that last for about an hour. The proposed mechanism for this effect is the creation of oxygen vacancies in the semiconductor that would create a path for charge transfer between the analyte and the nanoparticles. However, this hypothesis has never been confirmed experimentally. Furthermore, the tested structure of the PIERS substrate has always been composed of plasmonic nanoparticles on top of the semiconductor. Inhere we present PIERS results obtained on gold nanoparticles co-deposited with porous TiO_2 which confer them a unique position half buried in the semiconductor. The resulting PIERS intensity is among the highest measured until now but most importantly the duration of the effect is significantly longer (at least 8 days). Cathodoluminescence measurements on these samples show for the first time that two distinct

mechanisms are at stake for co-deposited and dropped casted gold nanoparticles. The oxygen vacancies hypothesis tends to be confirmed for the latter, but a the narrowing of the depletion zone explains the long PIERS effect.

1 Introduction

Surface Enhanced Raman Spectroscopy (SERS) is known for its high sensitivity and has been widely applied to the detection of biomarkers and molecules [1–5]. Researchers have reported enhancing factors up to 10^{14}[6–8] and some even claim that it is possible to detect a single molecule[9,10]. The understanding of the origin of SERS allow to go further than the simple detection of chemicals. For example, the study of the conformation of complex molecules[11,12] has been made possible because it is known that the Raman scattering enhancement is dependent on the distance from the enhancing surface. As a consequence, the closest to the surface a molecular bond is the strongest enhancement it will have.

The SERS effect has been experimentally described for the first time in the 1970s when scientists noticed that the Raman spectra were much more intense if the molecules were in the vicinity of a rough metallic surface [13–16]. The origin of SERS continues to be explored until today, however it is commonly admitted that part of the extraordinary enhancement is due to the generation of an electromagnetic field near the molecule. In the first SERS experiment, a delocalized Surface Plasmon (SP) was involved. Localized Surface Plasmon (LSP) refers to the collective oscillation of the nanoparticle (NP) electronic cloud by the excitation of an incident light and are a much powerful tool to confine and manipulate the electromagnetic field of light at the nanoscale. This explains why most of the SERS related research of these past decades has been focused on SERS with metallic NPs. Another proposition has been made to explain the origin of SERS, the so-called chemical effect[17] takes place when a molecule is binding to a metallic nanoparticle and charge transfer is promoted between the molecule and the metal.

The materials of the surface and of the NPs, as well as the geometry of the system are of crucial importance to set up SERS. For example, the electromagnetic effect may be due to the LSP, yet the intensity of the electric field around the NP is related to its shape. The lightning-rod effect[18,19] takes place on sharp metallic nanostructure where the electric field is confined. This contributes to considerably enhance the Raman scattered intensity[20–22]. Another way to contribute to the electromagnetic field intensity is to confine it in between two close nanoparticles to form hot spots[23].

Similarly, it is possible to contribute to the chemical effect for an even greater enhancement of the Raman scattering intensity. In this case the choice of materials has consequences on the electron transfer pathways between the nanostructured surface and the chemical. Traditionally Ag and Au are preferred for the NPs because they are showing the most intense plasmons in the visible[24], their chemistry is well known and allow a large range of molecules to be grafted. Au especially doesn't oxidize and is probably the most use material for SERS. Another example

is given by semiconductors. The intensity of semiconductor's LSP is indeed weaker, yet the wide use of semiconductors in the industry makes them good candidates for a compromise between cost and gain[25,26].

When a molecule is grafted on a metal, electron transfers are likely to take place between the Highest Occupied Molecular Orbital (HOMO) of the molecule and the Fermi level of the metal. In semiconductors, electrons transfer occurs between the HOMO and the conduction band (CB) or between the valence band of the substrate (VB) and the Lowest Unoccupied Molecular Orbital (LUMO) of the analyte. In other words, the use of a semiconductor increases the numbers of possible charge transfer mechanisms. It is especially interesting as their band gap can be tuned, it is thus possible to promote a preferred process for charge transfer, the other or even adapt the transition to a specific wavelength.

Adding metallic NPs to a semiconductor has been demonstrated to be even more efficient for SERS. Plasmonic NPs can contribute to charge transfer in different ways presented in **Figure 1**. The Plasmon Induced Charge Separation (PICS) mechanism (**Figure 1a**) where the charges are excited in the NP (either interband transition or hot electron) and have enough energy to overcome the Schottky barrier between the metal and the semiconductor. Another way to transfer electrons from a metallic NP to the semiconductor is to take advantage of its plasmonic activity. In PRET (Plasmon Resonant Energy Transfer) the electromagnetic field emitted by the LSP induces a charge excitation inside the semiconductor (**Figure 1b**). Finally, SERS can take advantage of the photocatalytic effect where the electron is transferred from the semiconductor into the NP (**Figure 1c**).

The possibility of adding charges to the plasmonic NP widens the possibilities for SERS as the chemical effect is based on charge transfer between the nanostructured surface and the analyte whose Raman scattering is to be enhanced. The group of J. R. Lombardi has exploited the combinations offered by Ag NPs in TiO_2 to induce SERS by charge transfer[25]. In 2016, Ben Jaber et al. [27] have gone one step further by using UV light to irradiate Au NP drop-casted on TiO_2 rutile. The enhancement of the Raman intensity is about three times higher by Photo-Induced Enhanced Raman Scattering (PIERS) than with traditional SERS. The authors claim that UV illumination results in oxygen vacancies (V_O) formation in the TiO_2 whose energy level under the conduction band of TiO_2. It eases the charge transfer from V_O to the Au NPs and then to the molecule when the system is under the illumination of the Raman spectrometer (**Figure 1d**). Around 60 minutes later, the V_O are cured in air and the PIERS effect disappears.

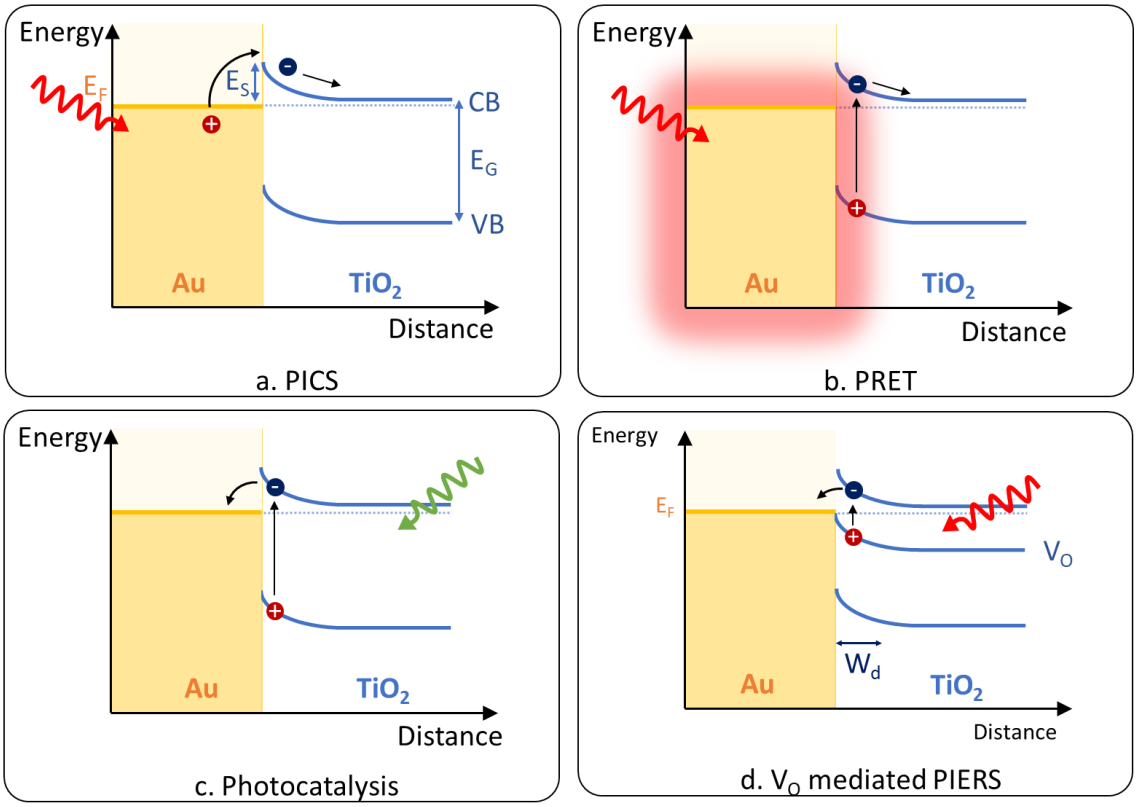

Figure 1. Mechanisms of charges transfer between a metallic nanoparticle and a semiconductor: a) PICS, b) PRET, c) Photocatalysis and d) Oxygen vacancy mediated PIERS. The Schottky barrier is described by E_F the Fermi level of the metal, VB and CB the valence and conduction band, E_G the energy of the band gap and E_S the energy of the Schottky barrier.

Since then, a few papers have reported results on PIERS. In all cases the NPs are on top of the semiconductor either by drop-casting a previously synthesized solution of Au or Ag NPs or by chemically synthesizing Ag NP directly on the semiconductor surface. So far quite a low number of systems have been investigated: TiO_2, ZnO and WO_3 are all semiconductors where the proposed mechanism of V_O formation upon UV irradiation has been advanced. In these systems, the wavelength of the LSP resonance (LSPR) is always blue shifted after UV irradiation. Other mechanisms have been considered in very specific systems, in 2018 Al-Shammari et al [28] have reported on their study of PIERS on Ag NP drop-casted on lithium niobate and, in 2020, Abid et al [29] have published their results of PIERS on Au NP drop casted on a 2D material, WS_2. In the first case, it seems that the Raman enhancement is favored by a photocatalytic effect. For WS_2 the authors suggest that the charge transfer is coming from the Au NPs toward the semiconductor and then to the analyte like what was propose in [30]. PIERS has already been demonstrated successful on a diversity of molecules: Raman probes[27–29,31], biomolecules (DNA[32], tyrosine[33], glucose[27]), explosives[27,34], and organic pollutants[35,36].

It has also been used for the study of V_O dynamics in semiconductors[37,38]. Nevertheless, this technique is still young and, as Zhao *et al.* are pointing out in their 2021's review[39], several issues must still be addressed. Among them, the optimization of the system "Semiconductor + NPs" and the study of the mechanisms of PIERS.

In the present paper we propose to focus on these two questions. Instead of drop-casted NPs, we are considering Au NPs that have been co-deposited together with the TiO_2, so they are embedded in the semiconductor (in the following they will be referred as "embedded Au-TiO_2"). For the first time we report on a red shift of the LSPR after UV irradiation and most importantly we observe a much stable enhancement (at least one week) than what was reported before. These results suggest that a distinct mechanism is at stake, therefore we have performed cathodoluminescence (CL) measurements to support our hypothesis on charge transfer mechanism specific to this system. Eventually a comparison of CL results with conventional drop casted Au NP is done to highlight the different possible processes of PIERS.

2 Results and discussion

2.1 TiO_2 growth and structure characterization

The embedded Au-TiO_2 was grown by the co-deposition of Au and TiO_2 with laser ablation (see experimental for the growth details and Bricchi et al. [40] for the characterization). The samples investigated here were obtained after annealing them at 700°C in air. The characterization of the sample morphology was conducted through SEM, on both embedded Au-TiO_2 (**Figure 2**) and bare TiO_2[40] films (i.e. without Au) before and after the annealing treatments. Synthetized films, in the as deposited conditions, presented a characteristic hierarchical 1D vertically oriented, tree-like nanostructure with very large specific surface area[41]. The thermal treatment did visibly affect the shape and dimensions of these nanostructures as the tree-like TiO_2 looked more compact. One of the consequences of this is the enlargement of the distance between the tree-like structure making the AuNPs more accessible. The annealing also impacts the size of the Au NP as their sized is going from about 5 nm before annealing to around 12 nm after. Figure 2d shows that the AuNPs are positioned in the bulk of the sample and on the surface of the TiO_2 tree-like structures. AuNPs are actually pinned to the surface of the trees which makes interactions possible with both TiO_2 and the environment.

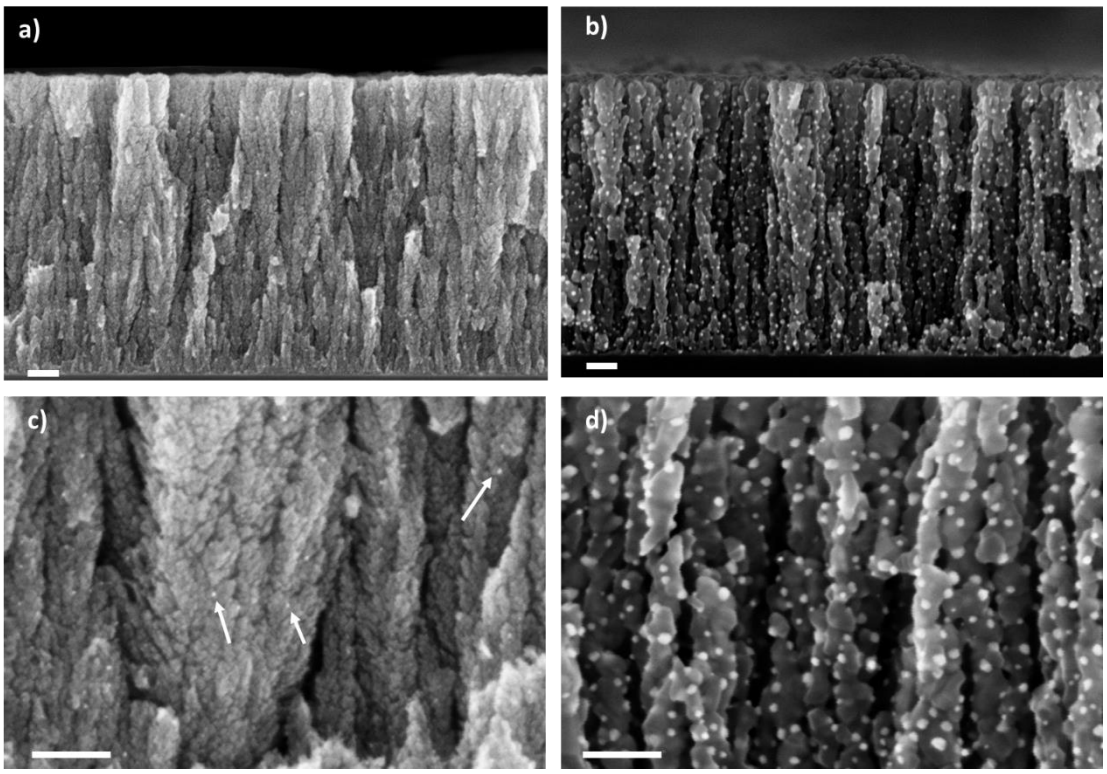

Figure 2. SEM images of the embedded Au-TiO_2 before a) and after b) annealing at 700°C. c) and d) are magnifications of respectively a) and b). The scale bar stands for 100 nm

Raman analysis was performed in order to investigate TiO_2 crystal structure. Anatase is well known to present six Raman active modes namely at 144 cm^{-1} (Eg), 197 cm^{-1} (Eg), 399 cm^{-1} (B1g), 519 cm^{-1} (superimposed with the 515 cm^{-1} band) (A1g, B1g) and 639 cm^{-1} (Eg). Rutile phase, instead, has five Raman active modes at: 143 cm^{-1} (B1g) 240 cm^{-1} (multi-photon process) 447 cm^{-1} (Eg) 612 cm^{-1} (A1g) and 826 cm^{-1} (B2g). **Figure 3** shows the Raman spectra obtained with an excitation wavelength of 514.5 nm and 633 nm; both spectra have been normalized to the intensity of the 144 cm^{-1} peak. The spectra acquired with the green excitation shows a very intense peak at 144 cm^{-1} and weaker peaks at 399 cm^{-1}, 519cm^{-1} and 639 cm^{-1}. The spectra acquired with an excitation wavelength of 633 nm displays the same peaks, however as it is less noisy new peaks can be identified 233 cm^{-1}, 450 cm^{-1}, 615 cm^{-1}. These peaks are characteristics of a rutile phase. A very bright peak at 685 cm^{-1} is not conventional for TiO_2, other data (not shown) indicates that it is linked to the presence of the embedded Au NPs and the thermal treatment.

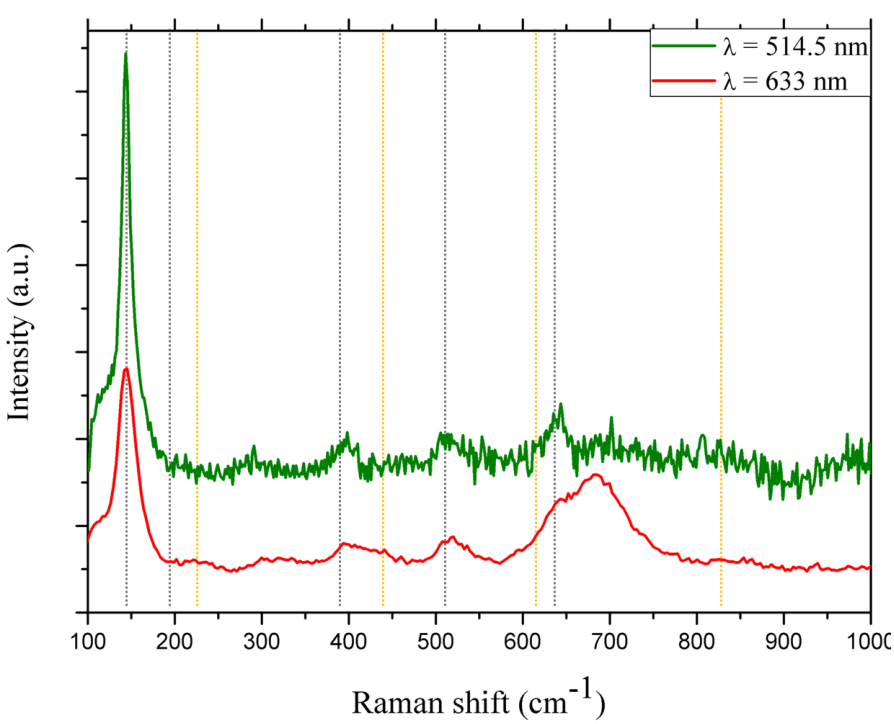

Figure 3. Raman of TiO_2 with Au NPs deposited at 8 Pa annealed at 700 °C. Spectra were acquired at 514.5 nm (green) and 633 nm (red). The gray dashed lines indicate the theoretical positions of anatase peaks and the yellow dashed lines the theoretical positions of rutile peaks

2.2 Optical properties

The extinction spectra of the samples have been measured before UV irradiation, immediately after and, at several times until one day (**Figure 4.**) after. These results are then used in the study of the influence of UV irradiation on the Raman intensity. The position of the peak before UV irradiation is 580 nm. Just after irradiation it has red-shifted to 609 nm and this position remains stable for almost two hours (**Figure 4b**). One day after the UV irradiation, the position of the LSPR is blue shifted but is still 14 nm greater that the original position. This is an important difference with other PIERS studies where the exposition to UV irradiation of a metallic NP/semiconductor system led to a blue shift. In the literature many combinations of materials have been tested for both the semiconductor and the plasmonic NPs. The size of the NPs as well as their growth process have also been varied. Among the parameters that have not been investigated yet is the position of the NPs with respect to the semiconductor (partially buried in the bulk instead of on top of the surface).

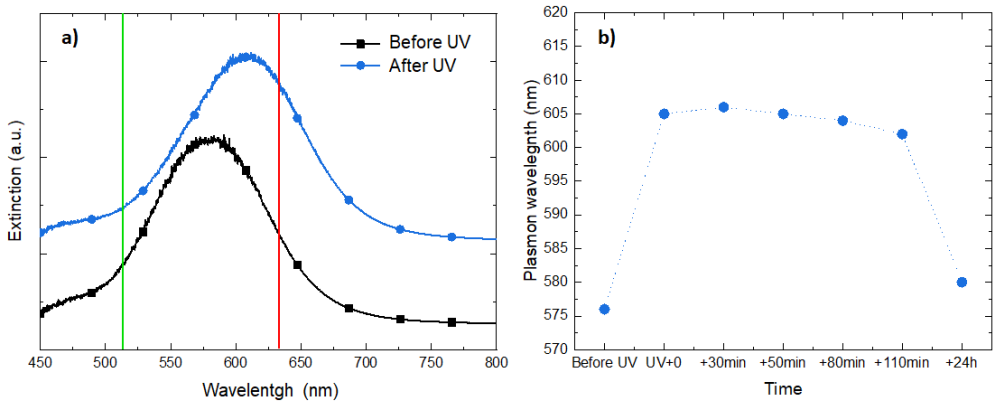

Figure 4. a) Extinction spectra of the sample acquired before UV irradiation (black) and immediately after (blue). The two vertical lines show the position of the laser excitations for Raman experiment. b) Evolution of the LSPR wavelength with time.

2.3 SERS measurement

The SERS measurements were performed after soaking the samples in a Mercaptobenzoic acid (MBA) solution. This molecule is a well-known Raman reporter whose SH group has a high affinity with gold but none with TiO_2, this guarantes a specific grafting on the Au NPs. A single layer of molecule is made sure by thorough rinsing[42–45]. SERS measurement were perfomered on a non irriadated sample and on another sample 30 minutes and 8 days after UV irradiation (30 minutes being the duration for the AuNPs functionalization, see experimental part) (**Figure 5**). On the three spectra the two broad peaks characteristics of MBA can be seen at 1080 cm^{-1} and 1590 cm^{-1} which are due to ring breathing modes, respectively in plane and axial. After irradiation these peaks are even more intense and weaker peaks emerge at 1184 cm^{-1} and 1486 cm^{-1} (CO and COO^- stretching).

Previously reported PIERS experiments dealing with MBA are not always successful to measure an enhancement of these two weaker peaks as compared with conventional SERS. The enhancement measured here may have several possible origins such as the distance of the CO and COO^- bonds from the surface of the Au NPs, or the properties of the AuNPs embedded in TiO_2 which could be more suitable for an enhancement of the chemical effect as it is demonstrated in the following.

The enhancement factor for SERS (EF_{SERS} – before UV) and PIERS (EF_{PIERS} – after UV) are calculated in a similar way as follow:

$$EF_{SERS} = \frac{I_{SERS} \cdot C_R}{I_R \cdot C_{SERS}} \quad (1)$$

$$EF_{PIERS} = \frac{I_{PIERS} \cdot C_R}{I_R \cdot C_{PIERS}} \quad (2)$$

Where I_{SERS}, I_{PIERS} and I_R stands for the SERS, PIERS and Raman intensity respectively. C_{SERS}, C_{PIERS} and C_R are the concentrations of MBA in each case. $C_R = C_{SERS} = C_{PIERS}$ as the functionalization does not depend on light. The PIERS gain is given by the comparison between EF_{PIERS} and EF_{SERS}:

$$G_{PIERS} = \frac{EF_{PIERS}}{EF_{SERS}} = \frac{I_{PIERS}}{I_{SERS}} \quad (3)$$

G_{PIERS} is summarized in **Table 1** and is of about one order of magnitude for the two main peaks at 1080 cm^{-1} and 1590 cm^{-1}. Furthermore, this enhancement is stable at least for 8 days after UV irradiation. For comparison G_{PIERS} is equal to 7.5, 9.0, 4.5 and 3.1 in, respectively, ZnO[31], WO_3[34], WS_2[29] and TiO_2[38] (with Au NPs drop casted on top) (for comparison with systems including AgNP a comprehensive table is available in [39]). In each of these cases the effect lasts for about one hour.

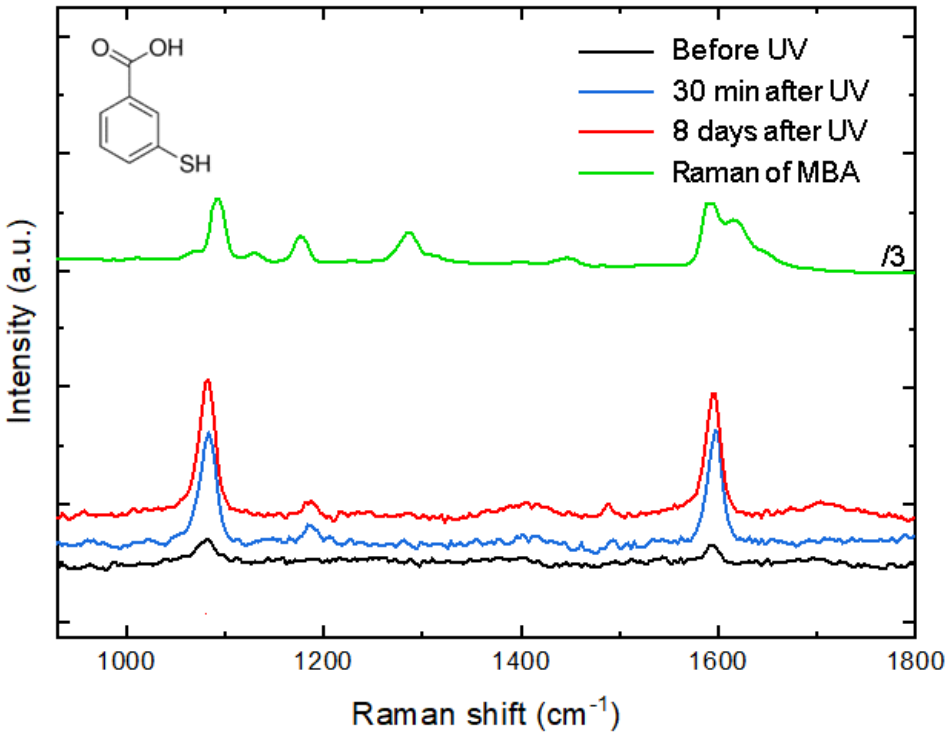

Figure 5. SERS spectra of MBA deposited on the samples before UV irradiation (black),30 minutes after UV irradiation (blue) and 8 days after UV irradiation (red). For comparison the Raman spectra of MBA powder divide by 3 is plotted in green, and the structure of MBA displayed in inset.

	1080 cm^{-1}	**1590 cm^{-1}**
Before UV	1	1
30 minutes after UV	10.2 ± 3.8	9.0 ± 2.6
8 days after UV	13.2 ± 4.4	8.8 ± 1.9

Table 1. G_{PIERS} measured at 1080 cm^{-1} and 1590 cm^{-1} as compared to the one obtained before irradiation.

2.4 Cathodoluminescence.

The results presented above confirm the finding of a Photo Induced Enhanced Raman Scattering (PIERS) effect. Even though the structure of the samples is very similar to what can be found in the literature the results are better in terms of enhancement and duration. We also observe a red shift of the LSPR when a blue shift is usually seen after UV irradiation which is a sign that UV irradiation does not affect the environment of the Au NPs in the same way as previously proposed.

To investigate the mechanism in the embedded Au-TiO_2, we have performed cathodoluminescence (CL) measurements on bare TiO_2 and embedded Au-TiO_2. In a CL experiment, an electron beam impinges a material and excite some energies transition. This results in the emission of photon at specific wavelengths that reveals charge recombination in the material. For example, as anatase bandgap is 3.2 eV, an emission is expected at the corresponding wavelength of 380 nm. CL is also able to excite charges in Au NPs, either interband transitions (from the d to the sp band) or hot electrons produced during the plasmon decay. All CL spectra below have been normalized to the 380 nm peak intensity to ease the comparison.

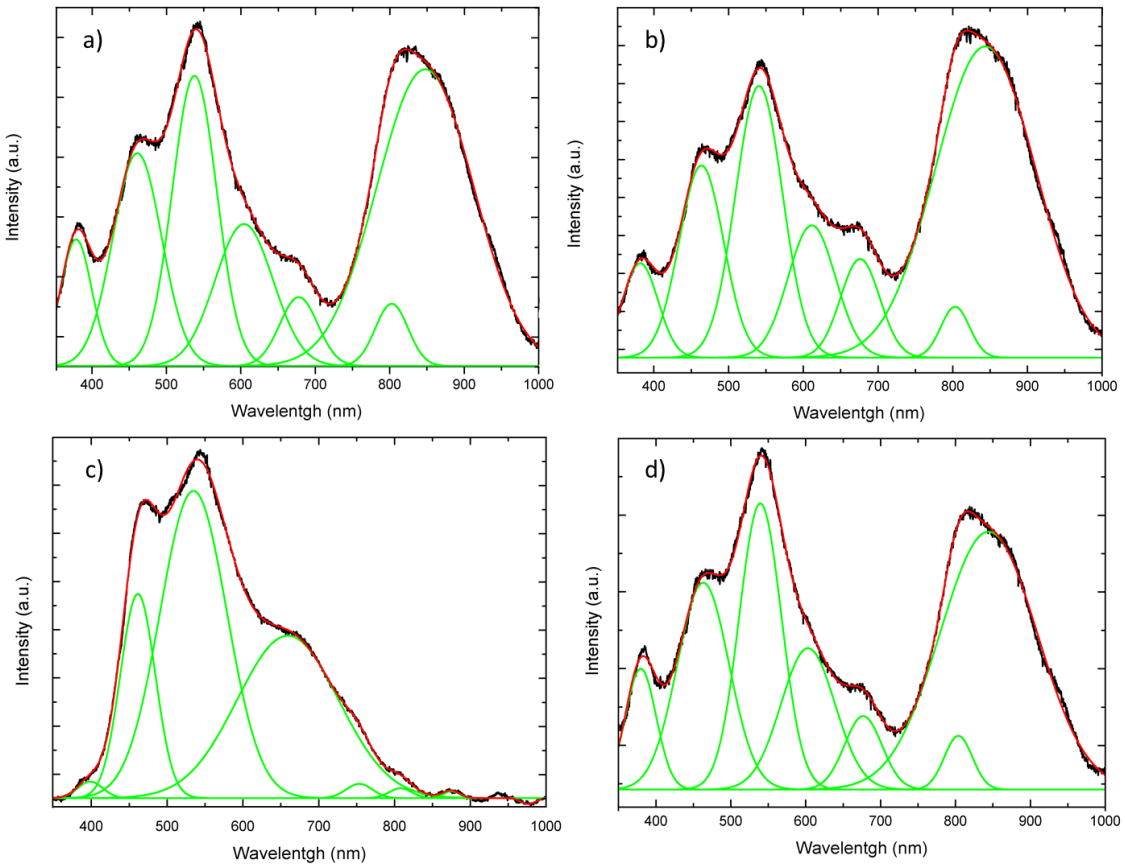

Figure 6. CL spectra of bare TiO_2 and embedded Au-TiO_2 before UV irradiation respectively a) and c) and immediately after UV irradiation respectively b) and d). The experimental data are plotted in black, deconvoluted peaks in green and the sum of these peaks in red.

Peak position (nm)	**Bare TiO_2 before UV**	**Bare TiO_2 after UV**	**Au-TiO_2 before UV**	**Au-TiO_2 After UV**
380	1	1	1	1
460	2.6	2.6	17.4	2.9
540	3.3	3.8	49.8	3.3
605	2.1	1.9	-	2.1
660	-	-	39.9	-
680	0.7	1.2	-	0.7
750	-	-	0.9	-
801	0.5	0.4	0.5	0.4
850	7.2	9.3	0.3	6.7

Table 2. Relative intensity of the CL peaks compared to the peak at 380 nm

2.4.1 CL of bare TiO_2

Figure 6a shows the CL spectrum of bare TiO_2 before UV irradiation. The deconvolution of the spectrum indicates the presence of seven peaks whose position and relative intensities are given in **Table 2**. The relative intensities are the ratio of the intensity of the peak under consideration to the one at 380 nm, this latter has been chosen as the reference since it corresponds to anatase bandgap. The large pattern in the infrared region is composed of two peaks: a weak one at 801 nm and another very bright at 850 nm. These two peaks are attributed to Ti^{3+} defects in rutile phase[46–48]: in presence of V_O two electrons are distributed to the adjacent Ti^{4+} ions becoming two Ti^{3+}. At the other end of the spectrum peaks attributed to anatase are found: 380 nm correspond to anatase band gap, 460 nm is attributed to self-trapped excitons and 540 nm is due to shallow traps ascribed to V_O. However, anatase presents a very bright peak at 520 nm when rutile does not[46,49] which is the case here. These first observations confirm the results of Raman spectroscopy: the crystalline structure of TiO_2 is made of both anatase and rutile. It also points out the presence of V_O already before UV irradiation.

After UV irradiation (**Figure 6b**), the structure of the spectrum is overall the same. However, one can notice slight changes in the intensity ratio between the peaks (**Table 2.**). Especially, the 850 nm luminescence is more intense than the one at 540 nm after UV irradiation. This is the sign of an increase in Ti^{3+} defects due to V_O formation[48].

2.4.2 CL of embedded Au-TiO_2

Before UV irradiation, the intensity ratio between the peaks of the CL spectra of embedded Au-TiO_2 (**Figure 6c**) is very different from bare TiO_2. **Table 2** shows more explicitly the differences: an increase by a factor 6.7 and 15 of the 460 and 540 nm peaks relative intensity; The shift of the peaks at 605 nm and 680 nm to the positions of 660 nm and 750 nm; the quenching of the peak at 800 nm and 850 nm.

The fact that the peaks in the IR have almost disappeared reveals the conservation of the Ti^{4+} ions. This mean either that there are less V_O in the TiO_2 and therefore less Ti^{3+}; or that the presence of Au prevents the charges let available by the V_O to be distributed to the Ti^{4+}.

At the same time, the peaks intensity at 460 nm and 540 nm have considerably increased. In CL, increased intensity is taking place only if there are more charge carriers that can recombine and consequently emit a photon.

The increase of the first peak demonstrates an increase of self-trapped exciton in the TiO_2 lattice.

The increase of the peak at 540 nm can have several origins. As mentioned above, they are

already found in bare TiO_2 where they are due to the shallow traps [50]. Another explanation could be related to PRET (**Figure 1b**) where the electromagnetic field generated by the LSPR promote charge transition in the TiO_2 bandgap. However, PRET is mostly taking place for NPs about 10 nm apart from the semiconductor surface which is not the case here. Another possibility would be a thermally activated mechanism. The temperature increases around the NP are less than 50 K[51] which is negligeable for accounting for the observations. Eventually, the enhancement can be attributed to PICS (**Figure 1a**). This effect takes place at the LSPR wavelength when Au NPs are in contact with the semiconductor. Here 540 nm is close to the LSPR position and also corresponds to the Au interband transition. In other words, CL electrons excites hot electrons in the Au NPs coming either from interband transition or LSPR, which have enough energy to overcome the Schottky barrier to be transferred at the V_O energy level[52]. In bare TiO_2 there is only one possible source of charge carriers in these regions of the spectrum whereas with the embedded Au-TiO_2 two more sources are available. More charge carriers implies more CL emission and explains the increase before UV irradiation.

The fact that the absence of Ti^{3+} coincides with the increase of self-trapped excitons suggests that the electrons left available by the V_O have not been redistributed to the Ti^{4+}. They are either transformed in self-trapped exciton or distributed to the Au NPs. This would explain the increase of the peaks at 460 nm and would be another source of luminescence at 540 nm.

The peak at 605 nm has shifted to 660 nm and has increased by a factor 20. The one at 680 nm has shift to 750 nm and has kept a similar intensity as the peak at 380 nm. These peak positions have already been reported in rutile powder. They are related to a lower number of radiative shallow traps[47]. The CL results on embedded Au-TiO_2 demonstrate the importance of the differences in the crystalline structure as compared to bare TiO_2. This, in turn, has consequences on the band diagram and charge transfer mechanism between Au and TiO_2.

Immediately after UV irradiation, the CL spectra of embedded Au-TiO_2 (**Figure 6d**) has significantly evolved and show high similarities with the spectra of bare TiO_2. The peaks relative intensities are very similar to what is measured in bare TiO_2. Especially the IR peaks are bright which is the sign of Ti^{3+} appearance. Another striking feature is the disappearance of the CL increase at 460 nm and 540 nm.

In the present experiment, PICS explains the CL increase before UV irradiation. How can this effect disappear afterwards? Other conditions for PICS to take place are that the Schottky barrier between the Au NP and TiO_2 has to be (i) high enough to be called a barrier (otherwise the contact would be ohmic, **Figure 7a**) but not too high so the LSPR energy is sufficient to overcome it and (ii) wide enough so back-transfer charges is not authorized (**Figure 7b**)[52].

After UV irradiation, LSPR red shifts from 580 nm to 609 nm (**Figure 4**). LSPR wavelength is further away from the shallow trap peak and PICS is less likely to happen. The LSPR shifts also means that the permittivity of the Au NPs surrounding medium is greater, in other words less charge carriers are available in the vicinity of the Au NPs, which is consistent with a decrease of the PICS effect (**Figure 1a**). The case of an ohmic contact between the Au NPs and the TiO_2 can also be excluded as it would allow charge transfer from the metal to the semiconductor. The decrease of the depletion zone width is more likely to explain our observations. Back-transferred charges is coherent with a red shift of the LSPR (less charges in the vicinity of the NP) and the decrease of the interband transition (the energy loss being accomplished via the TiO_2). The increase of Ti^{3+} defects is associated with an increase of V_O as the self-trapped excitons have decreased, we propose that part of these electrons is transferred to the Au NPs.

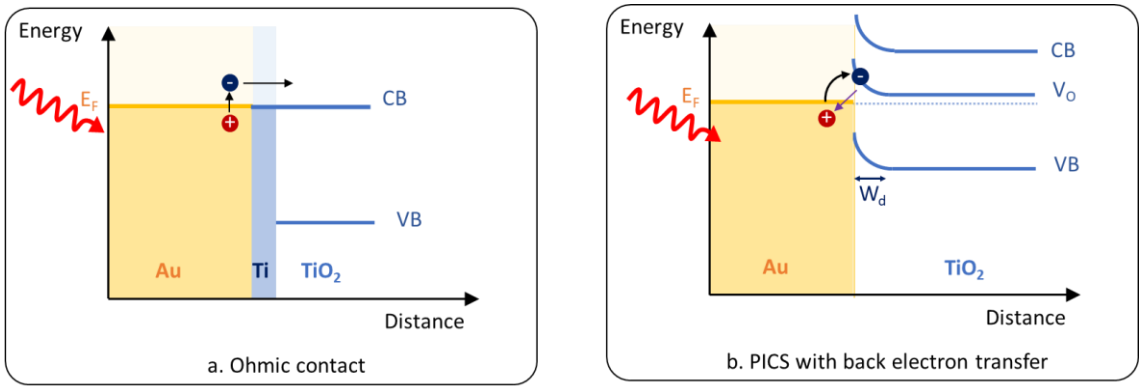

Figure 7: Proposed mechanisms for PIERS in embedded Au-TiO_2 a) Ohmic contact (no depletion zone) b) Back electron transfer in PICS with narrow depletion zone (Wd).

2.4.3 CL of Au NP drop-casted on the surface of TiO2

The literature so far has reported cases of PIERS using metallic NP on the surface of the semi-conductors. Typically, these NPs are synthesized in solution then a drop is deposited and dried on the semi-conductor. We have fabricated such samples for CL experiments before and after UV irradiation. The purpose is to demonstrate that two distinct mechanisms are at stakes when the Au NPs are co-deposited with the TiO_2 and drop-casted on the top of the TiO_2 surface.

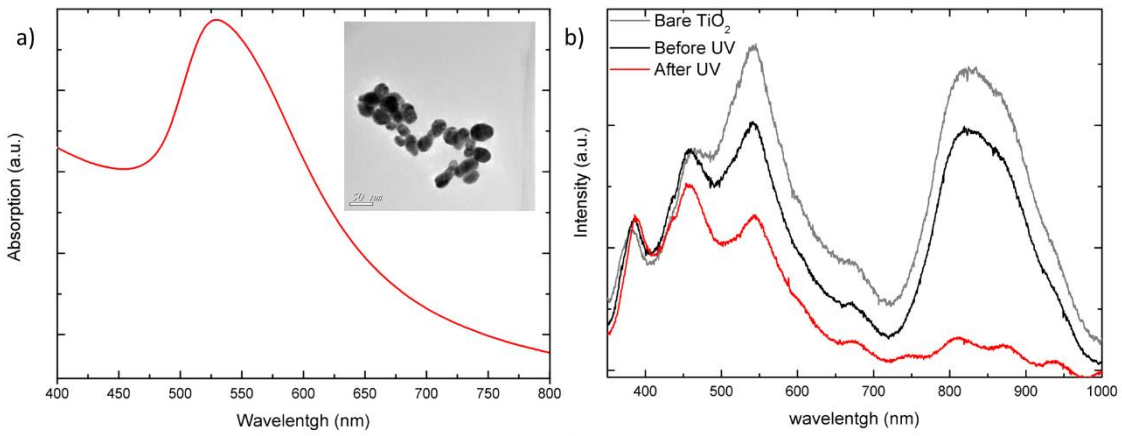

Figure 8. Au NP drop casted on top of TiO_2 surface a) TEM image and absorption spectra showing a peak at 527. b) CL spectra before and after UV irradiation, the CL spectra of bare TiO_2 is reminded for comparison.

Figure 8 shows a TEM image of the Au NPs drop casted on a carbon membrane. The absorption spectrum of this solution displays a peak at 525 nm which corresponds to the LSPR. **Figure 8b** show the CL spectra obtained before and immediately after UV irradiation on Au NPs drop casted on top of the bare TiO_2 which has already been described in the previous paragraph. Before UV, the spectrum is very similar to the one of bare TiO_2, although the intensity of the IR region and the 540 nm peak are less intense. After UV irradiation the intensity of the peaks at 540 nm has decreased and the IR region completely quenched.

Drop casted Au NPs are most sensitive to surface evolution of the TiO_2 structure as in this experiment the Au NPs are in contact with the top horizontal surface of the TiO_2. Giving the high absorption of TiO_2 in the UV, it makes sense that the density of V_O created by the UV is greater on the surface. However V_O are less mobile than Ti^{3+} which migrates inside the bulk[48]. As a consequence, CL peaks attributed to V_O will be more intense on the surface whereas those associated with Ti^{3+} will be found in the bulk. The quenching of the IR peaks here are explained by the fact that the Ti^{3+} defects are further away from the surface.

2.5 Mechanisms of PIERS

The enhancement in PIERS (**Figure 1d**) is based on the chemical effect where charges are transferred between the analyte and the nanostructured surface. Until now the proposed mechanism was based on charge injection from V_O in TiO_2 to Au NPs. This hypothesis is coherent with the CL results presented above for drop casted Au NPs: UV light induces V_O preferentially on the surface in position close to the Au NPs.

In the case of embedded Au-TiO_2, the position of Au NP partly buried in TiO_2 and partly available to MBA grafting imposes another mechanism. The analysis of CL and LSPR results suggests that the depletion zone width is narrower after UV irradiation. This is a consequence of V_O formation in the vicinity of the Au NPs. The unique position of the Au NPs in the TiO_2 allow them to be a reservoir of electrons from Ti^{3+} defects and then to transfer these charges into MBA. This, in turn, is enhancing the chemical effect of the surface enhanced Raman scattering. The defects produced in TiO_2 bulk are believed to be less mobile than those at the surface[53,54]. In other words, the duration of the PIERS effect is attributed to durable bulk defects local to the Au NPs.

3 Conclusions

In conclusion we have studied the PIERS effect on Au NP co-deposited together with TiO_2. The enhancement factor due to UV irradiation of the sample is increases by one order of magnitude which is among the highest values reported in the literature so far. CL experiments allowed us to conclude that this enhancement is due to a back transfer of charges which is typical of PICS in Shottky barrier with narrow depletion zone. The effect is stable in time contrary to what was previously reported thanks to the fact that the Au NPs are in the bulk and grown together with TiO_2. The CL analysis highlighted the differences between the mechanisms taking place when Au NPs are drop casted on the surface of the samples and when they are co-deposited with the TiO_2. In the first case, V_O are formed following UV irradiation, the energy level of the V_O is such that it is possible to excite electron transfer from TiO_2 to the Au NP with visible light, i.e. the laser used for the Raman scattering. In the second case, defects created by UV irradiation impact the width of the depletion zone and promote back-transfer charges to Au NP. This decreases the number of charges in the surrounding of the Au NPs and red shifts its LSPR. The enhancement of the Raman scattered intensity is possible thanks to the number of electrons in excess on the Au NP. These results demonstrate the influence of the growth mechanism on the PIERS effect. It would be interesting to study further the impact of the material on PIERS in a co-deposition process.

4 Experimental

4.1 Sample growths:

The co-deposition of Au-TiO_2 nanostructured films was realized with a composite target made of a TiO_2 target, on which three Au plates were attached, in order to reach a 2.9 % of Au coverage. Similarly, bare TiO_2 films were grown by ablation of a pure TiO_2 target without any Au plates. Target-to-substrate distance value was 5 cm. This condition represents the optimum in terms of interaction between ablated species and surrounding gas, because of low kinetic energy of the ablated species resulting in vertically oriented porous films. Deposition was carried out at room temperature at 8 Pa in oxygen atmosphere. Finally, the samples were annealed at 700 °C in air for 2 hours.

4.2 Scanning Electron Microscopy (SEM):

A field emission scanning electron microscope (FEG-SEM, Zeiss Supra 40) was used to perform morphological characterization analyzing films deposited on Si(100) substrate. Average size distribution of Au NPs was estimated through statistical analysis on SEM images with the open-source software ImageJ®.

4.3 Raman spectroscopy (Sample characterization).

Raman spectra were acquired with a Renishaw InVia micro Raman spectrometer, for the laser excitation wavelength of 514.5 nm (green) and Jobin-Yvon micro-Raman spectrophotometer (Labram 300) for the 633 nm wavelength. In both cases, the power was of 1 mW. The SERS spectra were recorded with the latter spectrometer, using a 100× magnification objective (NA = 0.90) in back-scattering geometry, with a spectral resolution of 3 cm^{-1} and a spatial resolution of about 1 µm for an acquisition time of 300 s. The typical peak of silicon at 521 cm^{-1} was used as an internal reference to normalize the intensities of all the spectra. The spectra presented here are the average of five spectra taken on different points of each sample, the details of the five spectra are available in the supplementary information file.

4.4 LSP measurements.

The LSPR position was measured thanks to extinction spectroscopy in transmission configuration with a 10x objective (NA=0.25) on an area of 100x100 $µm^2$ selected by the confocal hole of the Jobin-Yvon micro-Raan spectrophotometer (Labram 300) from which the edge filter was removed. The sample is illuminated was illuminated in normal incidence with collimated white light.

4.5 UV irradiation.

UV irradiation was performed under a UV bulb (λ = 254 nm) of power of 15 W and at distance of about 10 cm between the bulb and substrates, for 3 hours. The extinction spectra were measured immediately after the UV irradiation and at different time after up to one day.

4.6 Chemicals.

Mercaptobenzoic acid (MBA), and ethanol were purchased from Sigma Aldrich. MBA was diluted in ethanol at the concentration of 2.9 mM. Embedded Au-TiO_2 samples were then soaked in the solution for 30 minutes. Finally, they were thoroughly rinsed with ethanol before drying with nitrogen. The porosity of the film allowed MBA to penetrate along the whole TiO_2 film thickness.

The solution of Au NPs drop casted on top of the bare TiO_2 was synthesize using the Turkevitch methods which consist in reducing an $HAuCl_4$ salt with sodium citrate.

4.7 Cathodoluminescence.

The CL analysis have been performed with a Horiba HCLUE coupled with a scanning electron microscope ZEISS EVO MA15. The CL analysis have been made with an acceleration voltage of the electron beam of 10 kV. The measurement was performed before UV irradiation or immediately after.

5 References

[1] M. Cottat, N. Lidgi-Guigui, I. Tijunelyte, G. Barbillon, F. Hamouda, P. Gogol, A. Aassime, J.-M. Lourtioz, B. Bartenlian, M. L. de la Chapelle, *Nanoscale Res. Lett.* **2014**, *9*, DOI 10.1186/1556-276X-9-623.

[2] A. Brognara, I. F. Mohamad Ali Nasri, B. R. Bricchi, A. Li Bassi, C. Gauchotte-Lindsay, M. Ghidelli, N. Lidgi-Guigui, *Beilstein J. Nanotechnol.* **2020**, *11*, 1026.

[3] M. Cottat, C. D'andrea, R. Yasukuni, N. Malashikhina, R. Grinyte, N. Lidgi-Guigui, B. Fazio, A. Sutton, O. Oudar, N. Charnaux, V. Pavlov, A. Toma, E. Di Fabrizio, P. G. Gucciardi, M. Lamy De La Chapelle, *J. Phys. Chem. C* **2015**, *119*, 15532.

[4] D. Graham, R. Goodacre, *Chem. Soc. Rev.* **2008**, *37*, 883.

[5] N. Decorbie, I. Tijunelyte, S. Gam-Derouich, J. Solard, A. Lamouri, P. Decorse, N. Felidj, C. Gauchotte-Lindsay, E. Rinnert, C. Mangeney, N. Lidgi-Guigui, *Plasmonics* **2020**, *15*, 1533.

[6] C. David, N. Guillot, H. Shen, T. Toury, M. L. de la Chapelle, *Nanotechnology* **2010**, *21*, 475501.

[7] S. Nie, *Science (80-.).* **1997**, *275*, 1102.

[8] J. Aizpurua, H. Arnolds, J. Baumberg, I. Bruzas, R. Chikkaraddy, M. Chisanga, P. Dawson, V. Deckert, I. Delfino, B. De Nijs, G. Di Martino, J. Edel, H. Fleming, S. Gawinkowski, F. Giorgis, R. Goodacre, D. Graham, M. Hardy, C. Heck, S. Heeg, K. Hewitt, L. Jamieson, A. Keeler, A. Królikowska, C. Kuttner, N. Lidgi-Guigui, C. Lightner, J. Lombardi, S. Mahajan, N. Martín Sabanés, J.-F. Masson, N. S. Mueller, H. Muhamadali, K. Murakoshi, J. Popp, M. Porter, S. Reich, G. Schatz, Z.-Q. Tian, A. Tripathi, R. Van Duyne, X. Wang, A. Wark, K. Willets, M. Willner, *Faraday Discuss.* **2017**, *205*, DOI 10.1039/c7fd90088k.

[9] E. C. Le Ru, P. G. Etchegoin, M. Meyer, *J. Chem. Phys.* **2006**, *125*, 204701.

[10] C. J. L. Constantino, T. Lemma, P. A. Antunes, R. Aroca, *Anal. Chem.* **2001**, *73*, 3674.

[11] M. Iosin, V. Canpean, S. Astilean, *J. Photochem. Photobiol. A Chem.* **2011**, *217*, 395.

[12] M. Cottat, R. Yasukuni, Y. Homma, N. Lidgi-Guigui, N. Varin-Blank, M. Lamy De La Chapelle, C. Le Roy, *Sci. Rep.* **2017**, *7*, DOI 10.1038/srep39766.

[13] M. Fleischmann, P. J. Hendra, A. J. McQuillan, *Chem. Phys. Lett.* **1974**, *26*, 163.

[14] D. L. Jeanmaire, R. P. Van Duyne, *J. Electroanal. Chem. Interfacial Electrochem.* **1977**, *84*, 1.

[15] S. J. Lee, M. Moskovits, *Nano Lett.* **2011**, *11*, 145.

[16] M. Moskovits, *Rev. Mod. Phys.* **1985**, *57*, 783.

[17] A. Otto, in *Light Scatt. Solids IV. Top. Appl. Physics, Vol 54.* (Ed: G.G. Cardona M.), Springer, Berlin, Heidelberg, **1984**, pp. 289–418.
[18] P. F. Liao, A. Wokaun, *J. Chem. Phys.* **1982**, *76*, 751.
[19] M. B. Mohamed, V. Volkov, S. Link, M. A. El-sayed, *Chem. Phys. Lett.* **2000**, *317*, 517.
[20] J. Steidtner, B. Pettinger, *Phys. Rev. Lett.* **2008**, *100*, 1.
[21] T. Deckert-Gaudig, V. Deckert, *J. Raman Spectrosc.* **2009**, *40*, 1446.
[22] P. G. Gucciardi, M. L. de la Chapelle, N. Lidgi-Guigui, *Handbook of Enhanced Spectroscopy*, **2015**.
[23] A. Otto, *J. Raman Spectrosc.* **2006**, *37*, 937.
[24] C. F. Bohren, *Absorpt. Scatt. Light by small Part.* **1983**, DOI 10.1088/0031-9112/35/3/025.
[25] J. R. Lombardi, R. L. Birke, *J. Phys. Chem. C* **2014**, *118*, 11120.
[26] J. Kim, Y. Jang, N. J. Kim, H. Kim, G. C. Yi, Y. Shin, M. H. Kim, S. Yoon, *Front. Chem.* **2019**, *7*, 1.
[27] S. Ben-Jaber, W. J. Peveler, R. Quesada-Cabrera, E. Cortés, C. Sotelo-Vazquez, N. Abdul-Karim, S. A. Maier, I. P. Parkin, *Nat. Commun.* **2016**, *7*, 12189.
[28] R. M. Al-Shammari, M. A. Baghban, N. Al-Attar, A. Gowen, K. Gallo, J. H. Rice, B. J. Rodriguez, *ACS Appl. Mater. Interfaces* **2018**, *10*, 30871.
[29] K. Abid, N. H. Belkhir, S. B. Jaber, R. Zribi, M. G. Donato, G. Di Marco, P. G. Gucciardi, G. Neri, R. Maâlej, *J. Phys. Chem. C* **2020**, *124*, 20350.
[30] L. Yang, X. Jiang, W. Ruan, J. Yang, B. Zhao, W. Xu, J. R. Lombardi, *J. Phys. Chem. C* **2009**, *113*, 16226.
[31] G. Barbillon, T. Noblet, C. Humbert, *Phys. Chem. Chem. Phys.* **2020**, *22*, 21000.
[32] T. Man, W. Lai, M. Xiao, X. Wang, A. R. Chandrasekaran, H. Pei, L. Li, *Biosens. Bioelectron.* **2020**, *147*, DOI 10.1016/j.bios.2019.111742.
[33] Z. Y. Ke, C. J. Tsai, P. H. Liao, K. V. Kong, *J. Phys. Chem. Lett.* **2020**, *11*, 7443.
[34] D. Glass, E. Cortés, S. Ben-Jaber, T. Brick, R. Quesada-Cabrera, W. J. Peveler, Y. Zhu, C. S. Blackman, C. R. Howle, I. P. Parkin, S. A. Maier, **2019**, 13.
[35] M. Zhang, T. Chen, Y. Liu, J. Zhu, J. Liu, Y. Wu, *ChemNanoMat* **2019**, *5*, 55.
[36] M. Zhang, H. Sun, X. Chen, J. Yang, L. Shi, T. Chen, Z. Bao, J. Liu, Y. Wu, *ACS Sensors* **2019**, *4*, 1670.
[37] G. Barbillon, *Materials (Basel).* **2021**, *14*, DOI 10.3390/ma14164423.
[38] D. Glass, E. Cortés, S. Ben-Jaber, T. Brick, W. J. Peveler, C. S. Blackman, C. R. Howle, R. Quesada-Cabrera, I. P. Parkin, S. A. Maier, *Adv. Sci.* **2019**, *6*, DOI

10.1002/advs.201901841.
[39] J. Zhao, Z. Wang, J. Lan, I. Khan, X. Ye, J. Wan, Y. Fei, S. Huang, S. Li, J. Kang, *Nanoscale* **2021**, *13*, 8707.
[40] B. R. Bricchi, M. Ghidelli, L. Mascaretti, A. Zapelli, V. Russo, C. S. Casari, G. Terraneo, I. Alessandri, C. Ducati, A. Li Bassi, *Mater. Des.* **2018**, *156*, 311.
[41] L. Passoni, F. Ghods, D. Pablo, A. Agnese, M.-R. Javier, M. Ghidelli, G. Divitini, C. Ducati, M. Binda, S. Guarnera, A. Li Bassi, C. S. Casari, H. J. Snaith, A. Petrozza, F. Di Fonzo, **2013**, 10023.
[42] F. Schreiber, *Prog. Surf. Sci.* **2000**, *65*, 151.
[43] S. E. Creager, C. M. Steiger, *Langmuir* **1995**, *11*, 1852.
[44] M. C. Rodríguez González, P. Carro, E. Pensa, C. Vericat, R. Salvarezza, A. Hernández Creus, *ChemPhysChem* **2017**, *18*, 804.
[45] A. Brognara, I. F. M. A. Nasri, B. R. Bricchi, A. L. Bassi, C. Gauchotte-Lindsay, M. Ghidelli, N. Lidgi-Guigui, *Beilstein J. Nanotechnol.* **2020**, *11*, DOI 10.3762/bjnano.11.87.
[46] R. Plugaru, R. Vasilco, J. Piqueras, A. Cremades, *Proc. Int. Semicond. Conf. CAS* **2003**, *2*, 327.
[47] R. Plugaru, A. Cremades, J. Piqueras, *Proc. Int. Semicond. Conf. CAS* **2005**, *1*, 51.
[48] I. Fernàndez, A. Cremades, J. Piqueras, *Semicond. Sci. Technol.* **2005**, *20*, 239.
[49] A. Naldoni, F. Fabbri, M. Altomare, M. Marelli, R. Psaro, E. Selli, G. Salviati, V. Dal Santo, *Phys. Chem. Chem. Phys.* **2015**, *17*, 4864.
[50] A. Naldoni, F. Fabbri, M. Altomare, M. Marelli, R. Psaro, E. Selli, G. Salviati, V. Dal Santo, *Phys. Chem. Chem. Phys.* **2015**, *17*, 4864.
[51] I. Tijunelyte, E. Guenin, N. Lidgi-Guigui, F. Colas, J. Ibrahim, T. Toury, M. Lamy De La Chapelle, *Nanoscale* **2016**, *8*, DOI 10.1039/c5nr09018k.
[52] T. Tatsuma, H. Nishi, T. Ishida, *Chem. Sci.* **2017**, *8*, 3325.
[53] B. P. Uberuaga, X. M. Bai, *J. Phys. Condens. Matter* **2011**, *23*, DOI 10.1088/0953-8984/23/43/435004.
[54] G. G. Marmitt, S. K. Nandi, D. K. Venkatachalam, R. G. Elliman, M. Vos, P. L. Grande, *Thin Solid Films* **2017**, *629*, 97.